High-efficiency and fast-response tunable phase grating using a blue phase liquid crystal

Jin Yan, Yan Li, and Shin-Tson Wu*

College of Optics and Photonics, University of Central Florida, Orlando, Florida 32816, USA

**Corresponding author: swu@mail.ucf.edu*

Received February 24, 2011; accepted March 16, 2011;
posted March 21, 2011 (Doc. ID 143194); published April 13, 2011

We demonstrate a tunable phase grating using a polymer-stabilized blue phase liquid crystal. Because of the electric-field-induced rectangularlike phase profile, a high diffraction efficiency of 40% is achieved. Moreover, this device shows submillisecond response time. The proposed tunable phase grating holds great potential for photonics and display applications. © 2011 Optical Society of America

OCIS codes: 160.3710, 050.1950.

Liquid crystal (LC)-based electrically switchable phase gratings have the advantages of low cost, light weight, and low power consumption. As a result, they have found applications in optical interconnects, beam steering, and three-dimensional displays. Based on the electric field configuration, the tunable phase grating devices can be divided into two groups. The first group employs a longitudinal electric field with patterned electrodes [1–3], and the second group utilizes a TE field with interdigitated electrodes [4–6]. However, with conventional nematic LCs, the diffraction efficiency is usually low (<30%) and the response time is relatively slow (>10 ms).

Recently, the polymer-stabilized blue phase liquid crystal (PS-BPLC) has emerged as a promising candidate for photonics and display applications [7–11]. It exhibits two major attractive features: (i) no alignment layer is required, which simplifies the fabrication process and reduces the cost, and (ii) the response time is in the submillisecond range, which is ~10 × faster than nematic LCs.

In this Letter, we demonstrate a tunable phase grating using PS-BPLC. This device shows a high diffraction efficiency and submillisecond response time. A simulation was carried out to explain the experimental results. Good agreement between the simulation and experiment is obtained.

The BPLC employed in this study is a mixture composed of nematic LC (65% Merck BL038) and chiral dopants (10% Merck CB15 and 25% ZLI-4572). This BPLC host was then mixed with monomers (4.4% C12A and 4.5% RM257) and a 0.7% photoinitiator to form the PS-BPLC precursor. The phase transition temperature of the precursor is ISO 46.7 °C BP 37.6 °C N* during the cooling process and N* 40.1 °C BP 47.2 °C ISO during the heating process, where ISO represents the isotropic phase and N* stands for the chiral nematic phase. The precursor was injected into an in-plane-switching (IPS) cell with an electrode width of ~10 μm, electrode gap of ~10 μm, and cell gap of ~7.5 μm, as shown in Fig. 1. Afterward, a UV curing process was performed at 39 °C for 30 min, with an intensity of 2 mW/cm^2. After UV stabilization, PS-BPLC was formed. Although a slight green–blue reflected color can be observed, the cell is transparent and optically isotropic for red light ($\lambda = 632.8$ nm).

Figure 1 shows the device configuration and the phase change profiles. At the voltage-off state (V = 0), the PS-BPLC is optically isotropic. Diffraction only comes from the index mismatch between the indium tin oxide (ITO) electrodes and the LC medium. Because the ITO layer is very thin (~40 nm), this diffraction effect is very small and can be neglected. As an electric field is applied, the LC director tends to align with the electric field because the host nematic LC has a positive dielectric anisotropy ($\Delta\varepsilon$). As a result, birefringence is induced. The induced birefringence can be described by the extended Kerr effect [12]:

$$\Delta n_{\mathrm{ind}}(E) = \Delta n_{\mathrm{sat}}\{1 - \exp[-(E/E_s)^2]\}, \qquad (1)$$

where Δn_{sat} stands for the saturated induced birefringence and E_s represents the saturation field. The induced

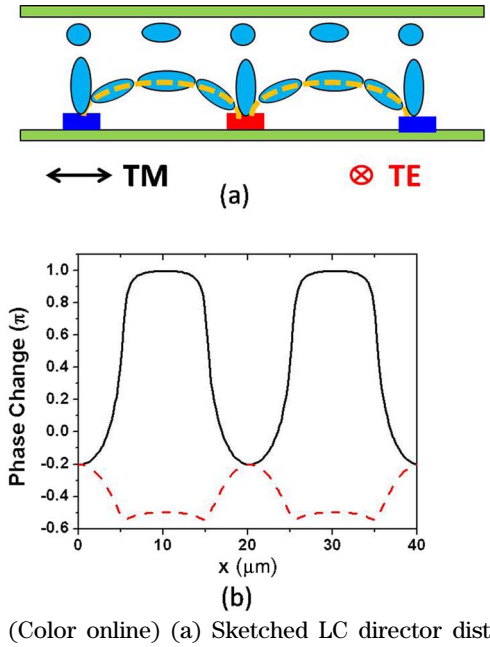

Fig. 1. (Color online) (a) Sketched LC director distribution and (b) corresponding phase profiles for TE (dashed curve) and TM (solid curve) polarized light under V = 160 V_{rms}.

ordinary and extraordinary refractive indices can be expressed by Eqs. (2) and (3), respectively [13],

$$n_o(E) = n_i - \Delta n_{\text{ind}}(E)/3, \tag{2}$$

$$n_e(E) = n_i + 2\Delta n_{\text{ind}}(E)/3. \tag{3}$$

Here, n_i represents the refractive index at the voltage-off state. Because of the nonuniform electric field in the IPS cell, the LC director distribution is also not uniform. On top of the electrodes, the electric fields are vertical; both TE and TM polarizations experience the ordinary refractive index n_o, which is smaller than n_i. Therefore, the accumulated phase is decreased. On the other hand, at the gaps between the electrodes, TE and TM waves experience different refractive indices. As a result, the accumulated phase is increased for the TM wave because it sees n_e but decreased for the TE wave because it sees n_o. From Fig. 1, the TM wave has more phase change than the TE wave. Therefore, we will focus only on the TM wave in the following discussion.

Figure 2(a) shows the experimental setup for optical measurement. The polarizer was used to select the TM-polarized light. An iris was placed behind the prepared sample to select the diffraction orders. The intensity of the diffraction orders was detected by a photodiode. At the voltage-off state, the diffraction effect is weak and the energy is mostly on the zeroth order, as shown in Fig. 2(b). Although the higher orders can be observed, the intensity is negligible as compared to that of the zeroth order. The sample was driven by a square-wave voltage with a 1 kHz frequency. As the applied voltage increases, the periodic phase distribution serves as a diffraction grating. As a result, the energy is transferred from the zeroth order to the first order, as Fig. 2(c) shows.

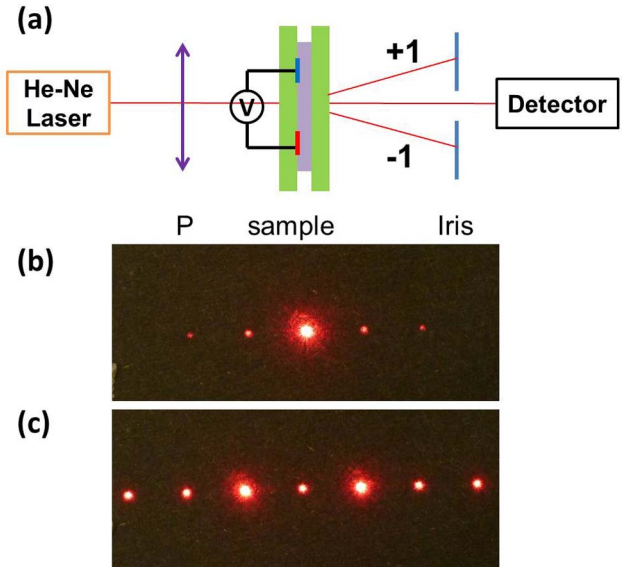

Fig. 2. (Color online) (a) Experimental setup for measuring diffraction efficiency. The iris can be relocated to select the diffraction order: P, polarizer. (b) Recorded diffraction patterns at the voltage-off state. (c) Diffraction pattern at 160 V. $\lambda = 632.8$ nm.

Figure 3 shows the diffraction efficiency of the zeroth, first, and second orders. The diffraction efficiency was calculated as a ratio between the intensity of diffracted order N and the total intensity at $V = 0$, described by Eq. (4):

$$\eta_N(V) = I_N(V)/I_0. \tag{4}$$

The diffraction efficiency is similar for the +1 and −1 orders, and both can achieve 40% at 160 V. This high efficiency is due to the reduced coherence length ξ of the PS-BPLC. For conventional nematic LCs, the LC director distribution does not exactly follow the electric field distribution, and it is usually smooth due to the long coherence length. With the polymer stabilization method, LCs are separated by the polymer network. As a result, ξ is greatly reduced. Therefore, the directors follow the electric field distribution, and a sharp spatial phase profile was obtained, as shown in Fig. 1. This rectangularlike phase profile helps improve the diffraction efficiency.

A simulation was carried out to fit the experimental data. First we calculated the electric field distribution in our IPS cell at the voltage-on states using the finite element method [14]. Next, for each applied voltage, the extended Kerr effect model [Eqs. (1)–(3)] was applied to calculate the induced n_o and n_e based on the electric field distribution. With the induced refractive indices, the phase profile can be calculated using Eq. (5):

$$\varphi(x) = \int_0^d n_e(x, z)\mathrm{d}z, \tag{5}$$

where d is the cell gap; z is normal to the substrate, and x is parallel to the substrate but perpendicular to the electrode direction. After, a Fourier transform of the phase profile was conducted to calculate the diffracted intensity of each order. The calculated result agrees quite well with the experimental data. The two fitting parameters are $\Delta n_{\text{sat}} = 0.2$ and $E_s = 14\,\text{V}/\mu\text{m}$. Compared with the host nematic LC, which has an intrinsic birefringence of 0.272 at 589 nm, the reduced Δn_{sat} is a reasonable value, because there are other components such as chiral dopants and polymers in this mixture.

Response times of the zeroth and first orders were also measured, as shown in Fig. 4. The solid black curve represents the zeroth order. As voltage of 170 V is applied, the transmittance is almost zero. Although the

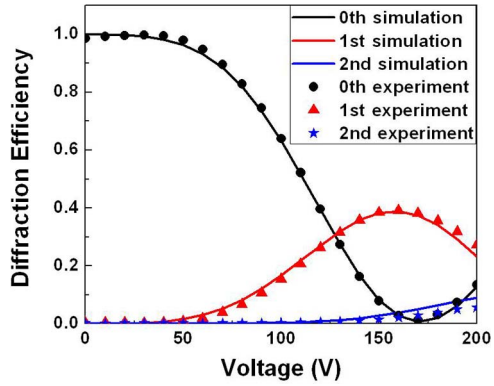

Fig. 3. (Color online) Diffraction efficiency of the zeroth, first, and second orders. Dots represent experimental data, and solid curves are the simulation results.

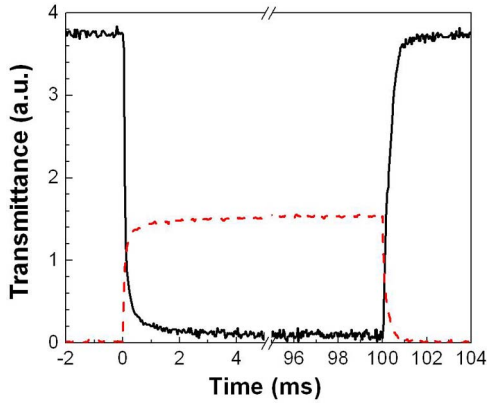

Fig. 4. (Color online) Measured response time of the zeroth (solid black curve) and first (dashed red curve) orders.

transmittance decreases, this process is still defined as the rise process. On the other hand, when the voltage is removed, the decay process takes place. The dashed red curve shows the response time for the first-order diffraction under 160 V, where the maximum efficiency occurs. The rise time and decay time are defined as 10% to 90% of the transmittance change. From Fig. 4, we find that the rise time is 360 μs and the decay time is 640 μs for the zeroth order. For the first order, the rise time is 560 μs and decay time is 480 μs. All response time is in the submillisecond range.

The only drawback for this tunable phase grating is the high driving voltage (160 V). However, with the development of the new blue phase materials, the driving voltage has been greatly reduced to 50 V [15]. On the other hand, with new device configurations, such as the one (B) proposed in [3], the driving voltage can be reduced from 160 to 95 V in order to achieve maximum diffraction efficiency for the first order.

In conclusion, we have demonstrated a tunable phase grating with a PS-BPLC composite. It is scatter free and does not need an alignment layer. High diffraction efficiency and submillisecond response time have been achieved at the expense of high driving voltage. With new materials and new device structures, the voltage could be greatly reduced. This device shows great potential for photonics and display applications, such as optical interconnects, beam steering, and projection displays.

The authors are indebted to the Industrial Technology Research Institute (Taiwan) and AU Optronics for financial support.

References

1. D. P. Resler, D. S. Hobbs, R. C. Sharp, L. J. Friedman, and T. A. Dorschner, Opt. Lett. **21**, 689 (1996).
2. M. Bouvier and T. Scharf, Opt. Eng. **39**, 2129 (2000).
3. L. Gu, X. Chen, W. Jiang, B. Howley, and R. T. Chen, Appl. Phys. Lett. **87**, 201106 (2005).
4. R. G. Lindquist, J. H. Kulick, G. P. Nordin, J. M. Jarem, S. T. Kowel, M. Friends, and T. M. Leslie, Opt. Lett. **19**, 670 (1994).
5. I. Fujied, Appl. Opt. **40**, 6252 (2001).
6. I. Drevenšek-Olenik, M. E. Sousa, G. P. Crawford, and M. Čopič, J. Appl. Phys. **100**, 033515 (2006).
7. H. Kikuchi, M. Yokota, Y. Hiskado, H. Yang, and T. Kajiyama, Nat. Mater. **1**, 64 (2002).
8. Y. Hisakado, H. Kikuchi, T. Nagamura, and T. Kajiyama, Adv. Mater. **17**, 96 (2005).
9. Z. Ge, S. Gauza, M. Jiao, H. Xianyu, and S. T. Wu, Appl. Phys. Lett. **94**, 101104 (2009).
10. L. Rao, Z. Ge, S. T. Wu, and S. H. Lee, Appl. Phys. Lett. **95**, 231101 (2009).
11. Y. H. Lin, H. S. Chen, H. C. Lin, Y. S. Tsou, H. K. Hsu, and W. Y. Li, Appl. Phys. Lett. **96**, 113505 (2010).
12. J. Yan, H. C. Cheng, S. Gauza, Y. Li, M. Jiao, L. Rao, and S. T. Wu, Appl. Phys. Lett. **96**, 071105 (2010).
13. J. Yan, M. Jiao, L. Rao, and S. T. Wu, Opt. Express **18**, 11450 (2010).
14. J. Jin, *The Finite Element Method in Electromagnetics* 2nd ed. (Wiley–IEEE, 2002).
15. L. Rao, J. Yan, S. T. Wu, S. Yamamoto, and Y. Haseba, Appl. Phys. Lett. **98**, 081109 (2011).